IEEE Access
Multidisciplinary | Rapid Review | Open Access Journal

Received April 13, 2021, accepted April 23, 2021, date of publication April 26, 2021, date of current version May 4, 2021.

Digital Object Identifier 10.1109/ACCESS.2021.3075914

Partial Discharge Electrical Tree Growth Identification by Means of Waveform Source Separation Techniques

CARLOS MADARIAGA[1], (Student Member, IEEE), ROGER SCHURCH[2], (Member, IEEE), JORGE ARDILA-REY[2], (Member, IEEE), OSVALDO MUÑOZ[2], AND SEBASTIAN FINGERHUTH[1], (Member, IEEE)

[1]School of Electrical Engineering, Pontificia Universidad Católica de Valparaíso, Valparaíso 2362804, Chile
[2]Department of Electrical Engineering, Universidad Técnica Federico Santa María, Valparaíso 2390123, Chile

Corresponding author: Roger Schurch (roger.schurch@usm.cl)

This work was supported in part by the Agencia Nacional de Investigacion y Desarrollo (ANID) through Fondo Nacional de Desarrollo Científico y Tecnológico (FONDECYT) Projects under Grant 11181177, Grant 1200055, and Grant Fondo de Fomento al Desarrollo Científico y Tecnológico (FONDEF) ID19I10165; and in part by the Universidad Técnica Federico Santa María under Grant PI_L_18_19.

ABSTRACT Electrical trees are one of the main degradation processes leading to failure of high voltage polymeric insulation. Electrical trees grow under the effect of partial discharges (PD), which can be measured and analyzed for condition monitoring of electrical insulation. In this paper, techniques that are normally used for classification of PD and noise separation were explored in their ability to determine the stage of growth of electrical trees: Spectral Power Clustering Technique (SPCT), Time-Frequency (TF) maps and Chromatic Technique (CT). The techniques allowed to analyze PD signals captured in ultra-high frequency (UHF) range with an antenna during tree growth. Laboratory treeing-samples were made of epoxy resin and trees were generated at six different excitation frequencies: 0.1, 10, 50, 150, 250 and 350 Hz. The results showed that two parameters, part of SPCT and TF maps, were sensitive to the tree progression and showed a consistent relation with the length of the tree: the low-frequency power ratio and the equivalent bandwidth. These two parameters were selected to create a new map, proposed for the characterization of electrical tree growth, which is more consistent and robust than the original separation maps. It was found that the low-frequency content of PD pulses proportionally increased with tree propagation.

INDEX TERMS Chromatic technique, electrical trees, electrical insulation, partial discharges, source separation techniques, spectral power clustering technique, time-frequency.

I. INTRODUCTION

One of the main degradation mechanisms in high voltage polymeric insulation systems of electrical equipment is the formation of electrical trees inside the material [1], [2]. Fundamentally, electric trees can be considered as microscopic tubular structures composed of gas channels that branch beyond their place of origin, eroding the insulation and causing equipment failure [1]. As is well known, the growth of electric trees is associated to internal PD activity that takes place in the areas where these channels or branches are formed. In this regard, PD measurement has proven to be a useful tool when studying the growth and evolution of this complex degradation phenomenon [1], [3]–[5].

Physically, PD activity is evidenced by the presence of short duration, low energy transient current pulses, which can be captured using detection impedances that are electrically coupled using standard measurement circuits [6], [7]. On the other hand, the electromagnetic radiation (EM) originated from PD can also be captured using very-high frequency (VHF) sensors, accurate in the range of 30–300 MHz, and ultra-high frequency (UHF) antenna-sensors, accurate in the range of 300–3000 MHz [7], [8]. One of the main advantages of using VHF-UHF sensors is the feasibility of capturing PD activity without requiring galvanic contact with the equipment being monitored.

The associate editor coordinating the review of this manuscript and approving it for publication was Pavlos I. Lazaridis.

In general terms, internal PD activity can be considered the most harmful type of PD for any insulation system since it is located within the material and therefore cannot be easily mitigated [9]. However, two other types of PD can act simultaneously during the measurement processes: corona and surface PD. Although these two types of PD can also contribute to deteriorate the insulation, once detected they can be more easily controlled during a scheduled maintenance of the asset [5].

In industrial environments, it is practically inevitable to capture relevant sources of noise with high-amplitude and frequency content similar to that of PD [10], [11]. This makes it more difficult to perform an accurate diagnosis of the insulation in an electrical asset since sources of great amplitude can be superimposed upon other sources of lower amplitude, whose origin could be related to an important degradation process or imminent failure [9], [10], [12], [13].

A strategy effectively used to address this problem is the application of separation techniques that allow grouping the signals that belong to the same type of source [14]. Normally, the separation process is carried out by means of clustering techniques based on mathematical analysis of the waveform of the acquired pulses. In this manner, it is possible to extract a series of characteristic parameters from each signal, which can be later represented in either two-dimensional or three-dimensional separation maps. The captured signals are located in specific areas of these separation maps according to the type of source they originate from. Once each cluster on the map has been established, the subsequent identification and diagnosis process can be carried out by simply analyzing each clustered source individually.

Among most-used separation techniques, the Spectral Power Clustering Technique (SPCT) [12], [13], time-frequency (TF) maps [9], [10], and chromatic technique (CT) [15] have proven to be efficient at differentiating multiple sources of PD from each other or from noise. One of the main advantages these techniques provide is the low computational burden since they are only based on the direct application of simple mathematical expressions. Furthermore, they do not require additional processing before or after the separation, as it happens with other separation techniques which require the prior use of noise filtering techniques on the signals to be classified [16] or the application of dimensionality reduction techniques such as principal component analysis (PCA) [17], [18], or t-Distributed Stochastic Neighbor Embedding (t-SNE) [19]. These techniques aim to reduce the number of parameters obtained so that the sources representation can be done in a 2D or 3D separation map.

In the technical literature, these separation techniques have been further studied, focusing on the variability that the generated clusters may have due to the dynamics of the defects being monitored. This analysis was detailed in [12] and [20], where it was possible to evidence that, for test objects that contained cylindrical vacuoles, the clusters represented in the separation map presented variations in their shape and position as the vacuoles increased their size. Furthermore, these separation techniques have demonstrated that the shape and position of the clusters associated with any type of source may vary significantly if there is any change in the electrical parameters of the measurement circuit, which also includes the test object [9], [10], [12], [13]. Thus, it is expected that these techniques could be useful in both the diagnosis of insulation containing electrical trees given their dynamics, and the difficult task of evaluating the growth of trees [21]–[26]. Nevertheless, only one of these techniques (SPCT) has been explored so far in terms of its capability to determine the state of progression of electrical trees [20], [26]. The findings of that research showed that power ratio maps (SPCT) are sensitive to the growth of electrical trees, presenting a displacement of the clusters in a 2D map as the tree progressed.

In addition to the challenge of determining the deterioration state of the insulation of an asset, the problem of interpreting PDs under excitation frequencies different from power frequency is a relevant aspect in insulation condition assessment. On the one hand, harmonic components are present in power networks due to the increasing use of power converters and nonlinear loads. Such is the case of renewable energies just as solar and wind, which provide an important income of pollution in power networks [27]. On the other hand, very low frequency (VLF, typically 0.1 Hz) is currently used for diagnostic testing of power cables [4] and new methods of PD analysis are required for VLF testing [5], [26]. Few and recent studies have considered PD source separation maps for electrical tree characterization at different frequencies [24], [26]. However, they have not exploited the techniques addressed in this paper, which have proven to be useful in applications involving both high frequency and low frequency signals [28], and can be complemented with several measurement systems like VHF or UHF [9], [13], [26].

In this paper, the characteristic parameters that are used in the separation processes with SPCT, T-F maps and CT are studied with the aim of evaluating their response during the growth of electric trees in epoxy resin samples. For each experiment, the PD measurement process was carried out using a 5 cm monopole antenna located in the vicinity of the samples that contained each of the treeing processes. Likewise, six different excitation frequencies were used to evaluate the response of the techniques from 0.1 Hz to 350 Hz.

II. EXPERIMENTAL SETUP

A. CIRCUIT AND MEASUREMENT SYSTEM

As depicted in Fig. 1, the measurement process of the tree growth was carried out using a balanced circuit, according to IEC 60270 standard [6]. To generate high voltage at variable frequency, an amplifier (Trek 20 / 20C-HS, HVA) was used to generate voltage in the range of 0.1 Hz to 350 Hz frequency. A signal generator (SG) was used to generate the low voltage signal for the amplifier and a digital oscilloscope (DO) for monitoring that signal. The samples were fed through a limiting resistance (R_x of $\sim$400 kΩ) to protect the instruments in the event of a breakdown. A PD-free sample C_k and the

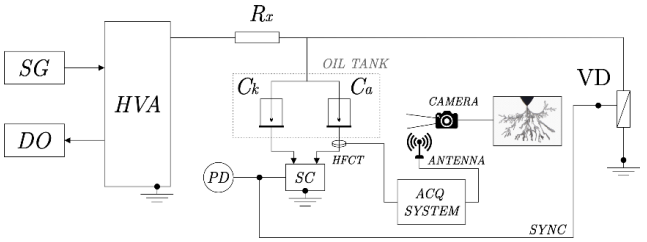

FIGURE 1. Circuit for electrical tree growth and monitoring.

treeing sample C_a, where the electric tree grows, were placed into a transparent container filled with silicone oil, in order to prevent unwanted surface discharges. Also, with the aim of minimizing the effect of external electrical noise, both samples were connected to a subtracting circuit (SC), following the strategy of the balanced circuit arrangement presented in the standard [6]. The output of the SC was connected into a commercial PD measurement system ('PD' in Fig. 1), as it is the conventional method to measure PD activity. These measurements were used for monitoring purposes only, but they were not included in the analysis presented in this work. Since the measurement system requires a sync signal from the voltage applied to the test object, a voltage divider (VD) was coupled to the output of R_x. For excitation frequencies of 10 Hz or higher, a capacitive VD with capacitance values of 50 pF and 0.033 μF was used. For VLF, a resistive VD was used, with resistance values of 9.9 MΩ and 100 kΩ.

Both C_a and C_k were made of epoxy resin (a DGBA epoxy system). C_a corresponded to the conventional needle-to-plane geometry with a distance gap of $\sim$2 mm between the needle tip ($\sim$3 μm tip radius) and the bottom-plane of the sample. C_k followed the same geometry except that the tip of the needle is semi-spherical rounded (radius of $\sim$0.5 mm). Electrical trees were generated and monitored in a test facility specially assembled for treeing experiments. An optical camera (DLSR Canon EOS T6 with a Canon EF 100mm f/2.8L macro lens) was used to take pictures every 5-30 seconds (depending on the applied frequency) during the growth process, in order to correlate the PD measurements with the tree progression.

Partial discharges were captured in UHF mode using an antenna. During the measurement process, a PXI high-speed acquisition system ('ACQ System' in Fig. 1) was used to digitize and store the waveform signals coming from a 5 cm monopole antenna located 25 cm from C_a. The PXI acquisition system used was composed by a NI PXIe-1071 chassis, a PXIe-5185 card and a NI PXIe-8135 controller. This acquisition system has two channels which can be configured to measure with a sampling frequency up to 12.5 GS/s, a bandwidth of 3 GHz and 8-bit resolution. In this work, the system sampling frequency was adjusted to 4 GS/s and the signals were acquired in time windows of 1 μs. Also, a commercial High Frequency Current Transformer (HFCT) was used to synchronize the signals captured with the monopole antenna in the acquisition system. The HFCT was placed between C_a and SC, and its output was connected to a 20 dB attenuator to protect the acquisition system in the case a relatively high signal is acquired, which normally occurs at insulation breakdown.

The monopole antenna used to capture EM emissions from PDs, was constructed from a 1.6 mm diameter copper wire, with a length of 5 cm and one of its ends attached to a 50Ω BNC straight bulkhead socket. A monopole antenna can be considered as a halved dipole which powers on its center line (relative to a ground plane) [8], [29], which has the main advantage of being easy to build and tune, allowing simple measurements in a specific frequency range [30], [31]. The capacity of monopole antennas, when measuring PD sources and electrical noise, has been extensively tested in other works [8], [29]–[31]. According to its dimensions, the implemented monopole antenna has a resonance frequency of 1300 MHz.

Fig. 2 shows the value of the return loss of the antenna (S_{11}), measured with a vector network analyzer (VNA Master MS2035B). It should be noted that S_{11} is related to the efficiency of the antenna and it is relevant when assessing the performance of the antenna.

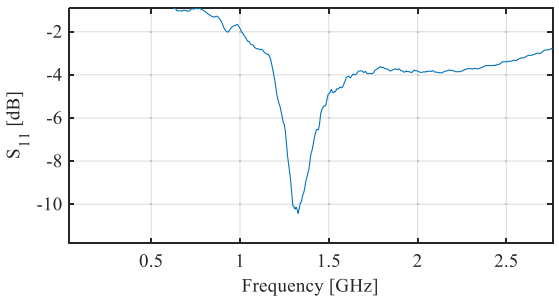

FIGURE 2. Measured S_{11} for the 5 cm monopole antenna.

B. ELECTRICAL TREE INITIATION AND GROWTH

The initiation and growth of the electrical trees were devised as two separated processes.

First, electrical trees for the samples C_k were initiated following a typical procedure of incremental steps of three minutes applying voltage with a constant RMS-value and constant frequency. The starting step was 10 kV - 50 Hz, then, the frequency or the voltage was increased until the voltage limit of the high voltage amplifier was reached; then, only the frequency could be increased. At any point of this initiation procedure, as soon as an electrical tree was visually detected, the voltage application was turned off. If no tree was initiated, the test sample was discarded as not suitable for treeing experiments. A set of samples with initiated electrical trees (treeing-samples) was created following this procedure to be ready for the electrical tree growth process.

Secondly, electrical trees were grown in six treeing-samples, each one of them energized with a different excitation frequency: 0.1, 10, 50, 150, 250 and 350 Hz, as presented in Table 1. The voltage was set to 12 kV for frequencies 50-350 Hz, 14 kV for 10 Hz and 16 kV for 0.1 Hz. The

TABLE 1. Energizing parameters of each treeing-sample.

Treeing-sample #	Frequency (Hz)	Voltage (kV)
1	0.1	16
2	10	14
3	50	12
4	150	12
5	250	12
6	350	12

applied voltage was higher in the lower frequency samples, otherwise the experiment was too long or the growth was imperceptible, especially in the case of 0.1 Hz.

In order to assure repeatability, another set of six treeing-samples was created and analyzed applying the same frequency and voltage. The results and tendencies were concordant among the sets and, for convenience, only one set of results is analyzed and discussed here as representative.

III. SEPARATION TECHNIQUES

Three separation techniques are exploited in this work for characterizing electrical tree growth. These techniques have been selected due to their ease of application, the low computational cost required during processing, and the performance they have demonstrated previously in their application in separating multiple sources of PD and electrical noise.

A. SPECTRAL POWER CLUSTERING TECHNIQUE

The SPCT requires to calculate the spectral power of the signals detected in two frequency bands: the low-frequency band, defined in the range $[f_{1L}, f_{2L}]$, and the high-frequency band, defined in the range $[f_{1H}, f_{2H}]$ [12], [13]. The spectral power of these two frequency bands is then normalized by dividing them by the total power of the detected signal. This procedure allows to calculate the power ratio for low frequencies (known as *PRL*) and the power ratio for high frequencies (known as *PRH*) as:

$$PRL = \frac{\sum_{f_{1L}}^{f_{2L}} |s(f)|^2}{\sum_{0}^{f_t} |s(f)|^2}, \tag{1}$$

$$PRH = \frac{\sum_{f_{1H}}^{f_{2H}} |s(f)|^2}{\sum_{0}^{f_t} |s(f)|^2}, \tag{2}$$

where $s(f)$ is the magnitude of the Fourier transform of the pulse signal $s(t)$, and f_t is the maximum evaluated frequency. The frequency bands can be chosen according to the observed spectrums. Thereby, each detected signal will have a *PRL* and a *PRH* value that are represented as a point on a separation map, called PR map [12].

Regarding the frequency intervals chosen, they could be complementary or overlapping. However, it is suggested that the concatenation of both frequency intervals do not cover the entire analyzed spectrum $[0, f_t]$ since in such a case the information of an axis would be redundant (0-*PRH* would be equal to 100-*PRL* and vice versa). Finally, f_{2L} should be less than f_{2H}, so as not to lose perspective of the represented interval [13].

The selection of the frequency bands associated to SPCT is a relevant methodological aspect since it defines the separation capability of the maps. Following the procedure described in [32], in this work the bands were adjusted to [0, 500] MHz for *PRL* and [500, 900] MHz for *PRH*. Likewise, f_t was set at 2 GHz according to the sampling frequency used during the acquisition process.

B. TIME-FREQUENCY MAPS

This technique is based on the time series transformation of PD signals and electrical noise into time sub-series corresponding to the similar waveform pulses [9], [10], [32]. This is carried out by taking the equivalent duration of the waveform (σ_T) and the equivalent bandwidth (σ_F) of the spectrum for each pulse and representing them by means of a two-dimensional map. To this end, the pulses of signals acquired are first normalized in the time domain as:

$$\tilde{s}(t) = \frac{s(t)}{\sqrt{\int_0^T s(t)^2 dt}}. \tag{3}$$

Then, the standard deviation of the normalized signal is calculated for both the time (4) and frequency (5) domains, which correspond to the equivalent duration (σ_T) and equivalent bandwidth (σ_F) of the signal respectively:

$$\sigma_T = \sqrt{\int_0^T (t - t_0)^2 \tilde{s}(t)^2 dt}, \tag{4}$$

$$\sigma_F = \sqrt{\int_0^\infty f^2 \, |\tilde{s}(f)|^2 \, df}, \tag{5}$$

where f is the frequency, $\tilde{s}(f)$ is the Fourier transform of $\tilde{s}(t)$ and t_0 is the "temporal gravity center" of the normalized signal, defined by:

$$t_0 = \int_0^T t \tilde{s}(t)^2 dt. \tag{6}$$

The parameter t_0 is used to make σ_T to be independent from the instant of time in which the PD is generated. Once the pulses have been characterized through σ_T and σ_F, these values are represented as points in a classification map, called TF map. This technique has demonstrated to be useful to classify different signal sources acting simultaneously into different clusters, in a way that each cluster represents the pulses associated to the PD source or the electric noise detected [9].

C. CHROMATIC TECHNIQUE

CT is a technique that allows the classification or differentiation of signals that are not easily identifiable in time or frequency [15], which is typical when analyzing pulses associated to the PD sources. In this paper, the classification of signals with this technique is implemented through three

different parameters: the energy content (E_b), average frequency (ω_c) and RMS bandwidth (B) of the signal, defined as:

$$E_b = \int_0^T |f(t)|^2 dt = \frac{1}{2\pi}\int_0^\infty |F(\omega)|^2 d\omega, \quad (7)$$

$$\omega_c = \frac{\int_0^\infty \omega |F(\omega)|^2 d\omega}{2\pi E_b}, \quad (8)$$

$$B = \sqrt{\frac{1}{E_b}\int_0^\infty (\omega - \omega_c)^2 |F(\omega)|^2 d\omega}, \quad (9)$$

where $F(\omega)$ is the Fourier transform of the signal $f(t)$, ω is the angular frequency and t is time. Note that B in (9) is slightly different from σ_F in (5), as the former calculates a normalized standard deviation centered in ω_c, whereas the latter derives the standard deviation centered in $\omega = 0$.

By means of these three parameters, a 3D map where each of the clusters is represented can be established. However, studies show that the parameters ω_c and B provide the best performance when separating simultaneous sources of PD and electrical noise [33]. For this reason, the parameter E_b was not used in this work.

IV. DATA MANAGEMENT

Electrical tree growth was characterized by both the waveform of PD pulses, measured through the entire tree growth, and the length of the electrical trees as they grew, extracted from pictures. Tree length is widely used for electrical treeing characterization [24], [26], and it is considered an appropriate parameter to estimate the remaining insulation life, since the final breakdown occurs soon after the tree crosses the insulation [34], [35]. The waveform of PDs and treeing pictures were synchronized for adequate correlation. The monitoring of the treeing-samples in which the trees were initiated and grew (see Table 1) generated a variable amount of data, which depended on PD dynamics and experiment duration. In this regard, the obtained data was normalized to analyze and compare results among treeing-samples. Due to the high number of measured PDs, the dataset generated in the monitoring of each treeing-sample was divided into three sub-datasets in order to group the data temporally, this is, with a temporal dependence. The first dataset contains the first third of the recorded PDs (Stage 1). The second subset contains the next third of PDs (Stage 2) and the third, the last PDs (Stage3). This PD grouping was chosen after a preliminary results analysis, constituting a simple and easily reproducible methodology to analyze the tendency of the parameters with respect to the tree growth. The generated maps that are presented in the next section therefore show one point per stage, which represents the centroid of the clusters obtained for that stage.

With the aim of evaluating the capability of the approached methods to determine the state of tree growth, in each stage the length of the growing electrical tree and the parameters obtained from the separation technique are calculated and correlated. Since each stage was conceived to have one third of all PD recorded in the monitoring of a treeing-sample and the growing process is non-linear and is different from treeing-sample to treeing-sample, the average tree length of each stage varies for different samples as well. In this paper, the average normalized tree length (l_{tree}) of each stage was estimated from treeing images recorded, and estimated according to:

$$l_{tree} = \frac{1}{N - M + 1}\sum_{i=M}^{N} \frac{l_i}{l_t}, \quad (10)$$

where l_i is the observed tree length in the i-th picture, as the furthest tree extent from the needle tip in direction to the ground plane, M and N are the number of the first and the last picture taken for a certain stage, and l_t is the final tree length in mm of the first branch that reached the ground plane, observed prior to breakdown. Therefore, l_{tree} can take values from 0 to 1, with 0 meaning that the tree has not yet grown, while 1 means that the tree is at maximum length, i.e. a tree branch has reached the counter-electrode, prior to breakdown. Table 2 groups the average normalized tree length for the three stages recorded from each treeing-sample.

TABLE 2. Estimated relative length of the tree for each stage.

Frequency (Hz)	Voltage (kV)	Stage 1 l_{tree1}	Stage 2 l_{tree2}	Stage 3 l_{tree3}
0.1	16	0.29	0.59	0.97
10	14	0.27	0.62	0.91
50	12	0.50	0.82	0.96
150	12	0.51	0.76	0.90
250	12	0.35	0.54	0.82
350	12	0.24	0.40	0.82

V. RESULTS AND ANALYSIS

In this section, the results of the application of SPCT, T-F maps and the CT to the recorded signals during tree growth are analyzed. As presented in Table 1, the results of the experiments shown in this section correspond to six treeing-samples energized each one with a different frequency: 0.1, 10, 50, 150, 250 and 350 Hz, which are named from (a) to (f) in the figures. The shape of the electrical tree structures varied depending on the applied frequency and voltage, consistent with what has been reported in the literature [24]. Nevertheless, in this work, the physical damage was characterized, and related to the recorded PD, through tree length. The tree growth was monitored for the entire experiment, and three different stages were defined as Stage 1 to Stage 3 and color coded in the figures.

A. MAPS OBTAINED BY MEANS OF SPCT

Fig. 3 shows the power-ratio maps obtained from the monitoring of the six treeing-samples. Fig. 3(a) also shows the image

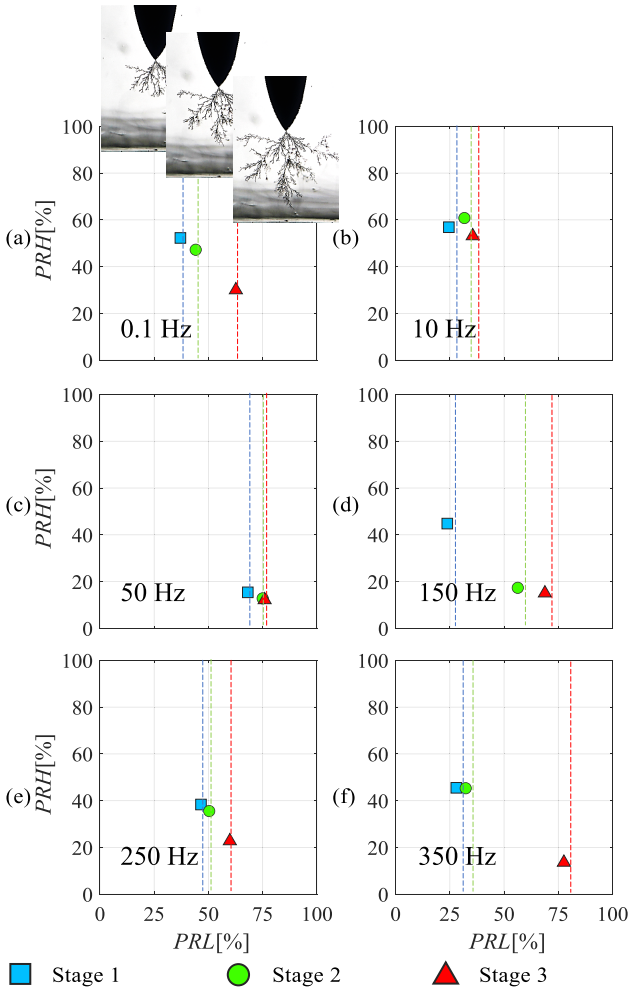

FIGURE 3. SPCT maps for treeing-samples energized with different frequency; (a) 0.1 Hz 16 kV, (b) 10 Hz 14 kV, (c) 50 Hz 12 kV, (d) 150 Hz 12 kV, (e) 250 Hz 12 kV, (f) 350 Hz 12 kV. Images of the tree at the end of each stage are shown for the 0.1Hz treeing-sample.

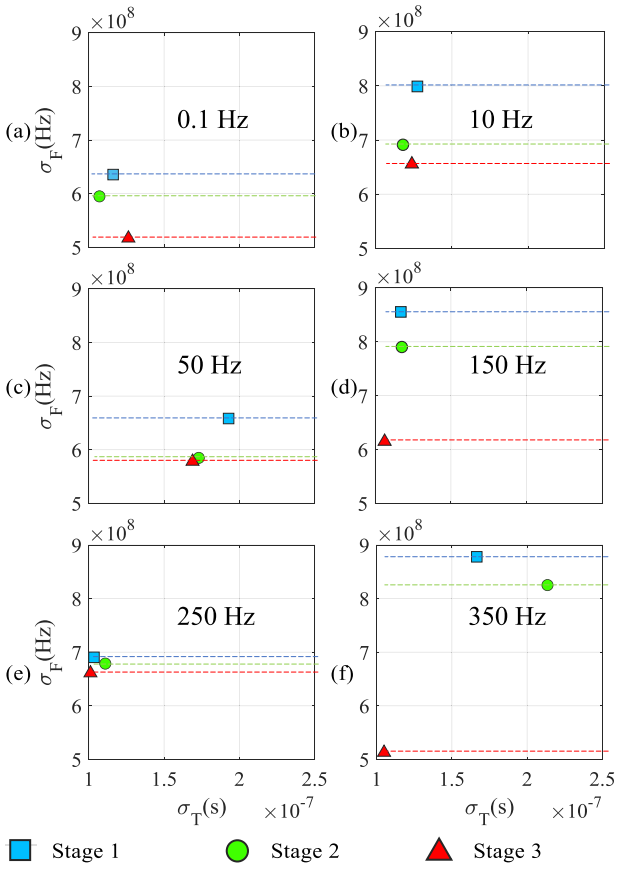

FIGURE 4. TF maps for treeing-samples energized with different frequency; (a) 0.1 Hz 16 kV, (b) 10 Hz 14 kV, (c) 50 Hz 12 kV, (d) 150 Hz 12 kV, (e) 250 Hz 12 kV, (f) 350 Hz 12 kV.

of the tree at the end of each stage of the 0.1 Hz treeing-sample to depict how the tree grows as the stages advance. The results showed that the centroid of the PR maps moved as the tree grew, indicating that SPCT is sensitive to the progression of the tree. Furthermore, in most of the cases it can be observed that the centroid moved from an upper-left position (Stage 1) towards a lower-right position (Stage 3), indicating that, in an early stage of tree-growth, the PD pulse waveform had a smaller low-frequency content than in a more advanced stage. For all the treeing-samples, the low-frequency power-ratio (*PRL*) increased as the tree grew, which can be easily seen by observing the vertical dashed guiding lines over each map. In turn, the high-frequency power-ratio (*PRH*) showed a non-monotonic tendency according as the stages advance, as it can be seen from the 10Hz treeing-sample results: *PRH* increases from the first stage to the second, whilst it decreases from the second to the third stage (ending at a level even lower than the first stage). Even still, the *PRH* value of the last stage was always lower than the value of the first stage for all six treeing-samples energized with different frequencies, which is, therefore, an indicator of either an energy increase on the lower frequency or an energy decrease in the higher frequencies.

B. MAPS OBTAINED BY TF TECHNIQUE

Fig. 4 shows the maps obtained using TF technique, in which the equivalent duration (σ_T) and equivalent bandwidth (σ_F) were calculated for each stage. From the results, it can be noted that σ_F proved to be sensible to the tree growth, as the first stage has the higher σ_F value, followed by the second and the third stage, configuring a monotonic tendency for all six samples. This can be best seen as a downward movement of the centroids in Fig. 4, as the horizontal dashed lines show. It can be observed that the equivalent bandwidth always decreased with tree evolution, suggesting a low-frequency energy increase or a high-frequency energy decrease, in concordance with SPCT results.

In contrast, the equivalent duration did not have a consistent tendency as the tree grew, since it did not always increase or always decrease with the evolution of the stages, therefore, σ_T is not suitable as a tree-growth indicator.

C. MAPS OBTAINED BY MEANS OF CT

Fig. 5 shows the CT maps obtained for the six treeing-samples. On the one hand, for most of the cases, the average bandwidth of each stage B did not show any consistent tendency, but only little variation, indicating that is not sensitive to electrical tree growth. On the other hand, the average frequency ω_c of each stage showed variation as the tree progressed, with most of the cases having a downward movement of the centroid in the map, as the horizontal dashed lines show. However, the variation of ω_c is less pronounced than the previously explored parameters PRL or σ_F. Also, the decrease was not monotonous for the 50 and 150 Hz treeing-samples.

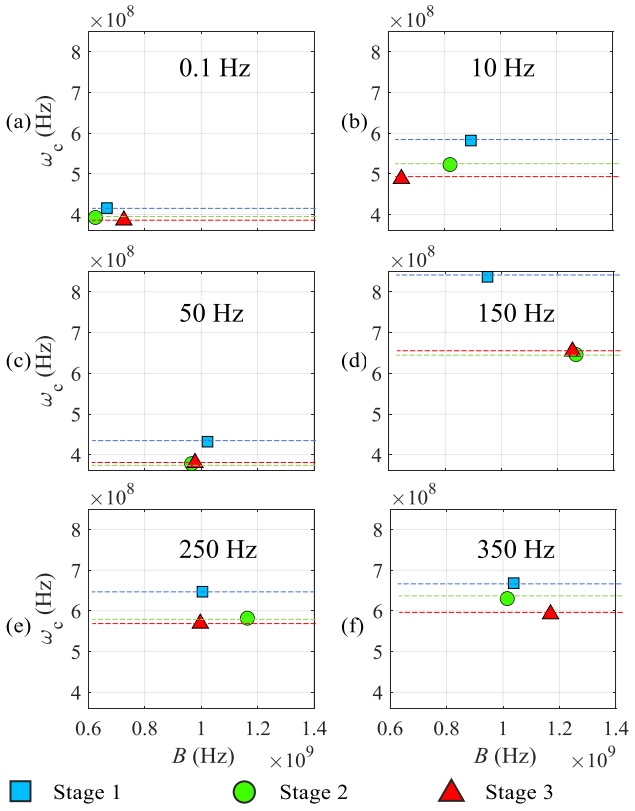

FIGURE 5. CT maps for treeing-samples energized with different frequency; (a) 0.1 Hz 16 kV, (b) 10 Hz 14 kV, (c) 50 Hz 12 kV, (d) 150 Hz 12 kV, (e) 250 Hz 12 kV, (f) 350 Hz 12 kV.

D. VARIATION OF PARAMETERS WITH TREE GROWTH

As previously analyzed, parameters PRL, σ_F and ω_c were the most sensitive to electrical tree growth, and thus, they were selected to further analyze their variation and relation with the degradation process of tree growth. Fig. 6 shows the variation of the selected parameters in function of the average normalized tree length, which was defined in (10).

From Fig. 6, it can be seen that PRL variation has a good agreement with the tree growing process for all six experiments, which is concordant with the preliminary findings of [26]. In most cases, although only three point-stages were

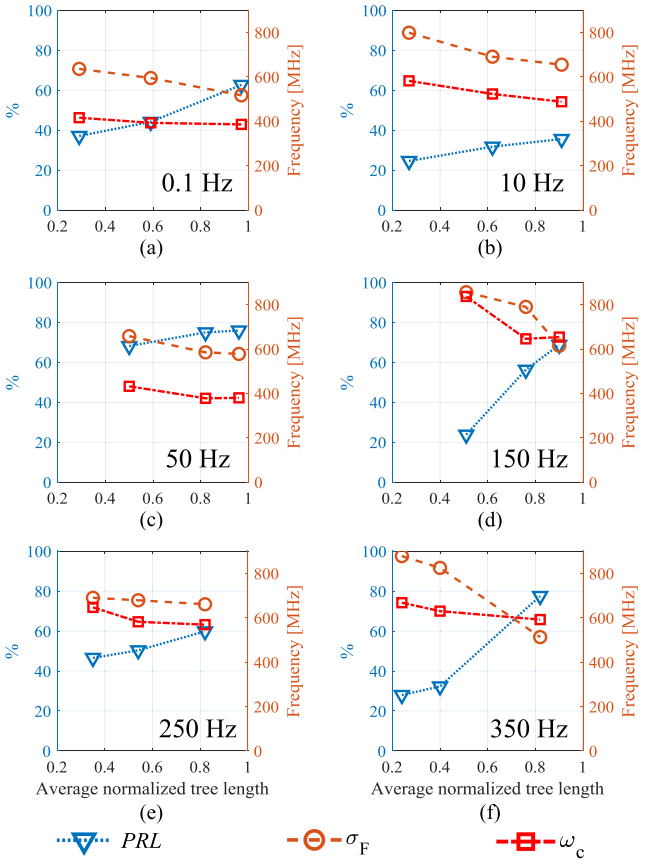

FIGURE 6. Value of relevant parameters as function of tree length for treeing-samples energized with different frequency; (a) 0.1 Hz 16 kV, (b) 10 Hz 14 kV, (c) 50 Hz 12 kV, (d) 150 Hz 12 kV, (e) 250 Hz 12 kV, (f) 350 Hz 12 kV.

analyzed, it can be noted that there was a proportional relationship between PRL and tree length. To complement this, σ_F (obtained from the TF technique) also showed a monotonic tendency with respect to tree length, since for all cases it decreased with tree progression. In turn, ω_c (derived from the CT) showed a less clear tendency related to the tree growing process.

The performance of these parameters can be further analyzed by means of the values presented in Table 3, which summarizes the difference of the parameters PRL, σ_F and ω_c between two consecutive stages. In order to assist the visualization of the variations, some values are highlighted for an easier identification of the tendencies. For instance, $\Delta l_{tree1-2}$ is the difference of the average tree length between the first and the second stage, and $\Delta l_{tree2-3}$ is the difference between the second and the third stage.

In the first treeing-sample (0.1 Hz), as $\Delta l_{tree2-3}$ was greater than $\Delta l_{tree1-2}$, then $\Delta l_{tree2-3}$ was highlighted. This is repeated for each parameter. In the cases where parameters did not show a monotonic tendency, the values were not highlighted, as was the case of $\Delta\omega_{c1-2}$ and $\Delta\omega_{c2-3}$ for the 50 and 150 Hz samples.

TABLE 3. Variation of relevant parameters between stages for all six samples.

(Hz)	(kV)	$\Delta l_{\text{tree1}-2}$ (%)	$\Delta l_{\text{tree2}-3}$ (%)	ΔPRL_{1-2} (%)	ΔPRL_{2-3} (%)	$\Delta\sigma_{\text{F1}-2}$ (MHz)	$\Delta\sigma_{\text{F2}-3}$ (MHz)	$\Delta\omega_{\text{c1}-2}$ (MHz)	$\Delta\omega_{\text{c2}-3}$ (MHz)
0.1	16	30	38	7	18	-41	-78	-23	-7
10	14	35	29	7	4	-108	-36	-59	-35
50	12	32	14	6	1	-73	-7	-54	2
150	12	25	14	32	13	-66	-175	-191	8
250	12	19	28	4	9	-11	-18	-65	-13
350	12	16	42	5	45	-53	-312	-38	-39

From Table 3, it can be firstly noted that *PRL* had both a monotonous tendency and a notorious relation with respect to the tree length for all six treeing-samples, as the results of each sample has similar response: In 0.1, 250 and 350 Hz samples, $\Delta l_{\text{tree1}-2}$ was smaller than $\Delta l_{\text{tree2}-3}$, which corresponds with ΔPRL_{1-2} being smaller than ΔPRL_{2-3}. In contrast, for 10, 50 and 150 Hz samples, $\Delta l_{\text{tree1}-2}$ was greater than $\Delta l_{\text{tree2}-3}$, which correlated with ΔPRL_{1-2} being also greater than ΔPRL_{2-3}.

In turn, σ_{F}, had a monotonous tendency for all six samples, and was related with tree length variations in five of the six treeing-samples, excluding the 150 Hz sample in which $\Delta l_{\text{tree1}-2}$ was greater than $\Delta l_{\text{tree2}-3}$, but $\Delta\sigma_{\text{F1}-2}$ was smaller than $\Delta\sigma_{\text{F2}-3}$.

Finally, ω_{c} showed a less notorious relation with tree length compared to the other two parameters: from the highlighted values of Table 3, it can be noted that only a third of the cases showed a consistent relation with tree length variation.

In summary, *PRL* and σ_{F} showed a consistent relation with the average normalized tree length since the variation of the parameters and the variation of the tree length between stages kept almost unchanged. This could suggest the existence of a proportional relationship between the parameters (specially *PRL*) and the tree length.

VI. DISCUSSION

A. MAPPING TECHNIQUES

From the obtained results, it can be firstly observed that the most responsive parameter with the tree growth was *PRL*, part of the SPCT, followed by the parameter σ_{F}, part of the TF technique, which showed a consistent response: for all six treeing-samples their value decreased as the tree progressed. However, *PRL* values strongly depend on the selected low- and high-frequency bands, while σ_{F} does not require any prior user-entry value. Nonetheless, the identified tendency of the evaluated parameters can be explained through SPCT results: PR maps showed the displacement of the centroids from the upper-left corner to lower-right corner as the tree grew. This meant that the spectrum of the detected PDs signals proportionally increased its energy in the low frequencies (lower than 500 MHz – *PRL* range), at the expense of an energy decrease in the high frequencies (higher than 500 MHz – *PRH* range). As the energy of the low-frequency interval increased with respect to the total energy, then the equivalent bandwidth σ_{F} consequently decreased (σ_{F} is defined as the frequency-based standard deviation, centered in $\omega = 0$ and should be sensitive to spectrum variations).

In turn, the tendency of ω_{c}, obtained by means of CT, partially confirms this statement: while the tree grew, the average frequency decreased, which was related to an increase of the relative energy in the low-frequency bands. Notwithstanding, parameter ω_{c} was less effective as a descriptor of electrical tree growth. This was noted from the non-monotonic tendency of ω_{c} with respect of the tree length, for the 50 and 150 Hz treeing-samples. The evaluation of ω_{c}, as defined in (8), requires the computation of E_{b}, which has been stated to not be suitable for PD source separation [33]. Table 4 groups the average energy of the PD signals for the three stages of all six treeing-samples. From the Table 4, it can be noted that E_{b} does not provide a good response to the tree growth either, which in turn undermines the feasibility of ω_{c} of being a good descriptor of tree growth. Note that, in (8), the numerator of the expression is similar to (5), and so the response of both terms (ω_{c} and σ_{F}) to tree progression should be similar if it were not for the consideration of E_{b} in (8).

TABLE 4. Average energy of detected signals of each stage.

Frequency (Hz)	Voltage (kV)	Stage 1 E_{b1} (μJ)	Stage 2 E_{b2} (μJ)	Stage 3 E_{b3} (μJ)
0.1	16	39.21	72.04	38.56
10	14	3.69	3.20	8.69
50	12	2.76	12.54	19.97
150	12	2.30	6.41	0.77
250	12	0.71	1.27	4.32
350	12	7.67	5.15	3.40

The equivalent duration σ_{T} did not show a consistent tendency when mapped by means of TF technique. By analyzing (4), it can be seen that σ_{T} is related to the dispersion of the signal data around the 'temporal gravity center' t_0, which should be near the instant in which the peak of the signal is achieved. This dispersion around the peak of the signal configures a time band that is usually interpreted as the equivalent duration of the signal. As shown from the results of σ_{T} for the six samples, this representative time band of the PDs was not related to the state of tree growth. In turn, *PRH* showed a non-monotonic tendency according as the tree grew, as noted from the 10Hz treeing-sample results. However, the

PRH value in the third stage was always lower than the first stage for all six treeing-samples. This suggests that the PDs recorded in the last states of growth have a proportionally lower high-frequency energy content than the PDs recorded at the beginning of the treeing process.

In brief, changes of the propagation media of detected PD signals, due to carbonization of tree channels when the tree grows, translates into variations of the waveform and the energy content of the spectrum of detected PDs. These changes can be best detected by *PRL* and σ_F, which proved to be proportionally related to changes of the state of tree progression.

B. PROPOSED MAP FOR ELECTRICAL TREEING CHARACTERIZATION

Parameters *PRL* and σ_F showed promising results as descriptors of electrical tree growth by evidencing a consistent tendency in relation to the average normalized tree length. Therefore, a 2D map combining both parameters was devised, as shown in Fig. 7.

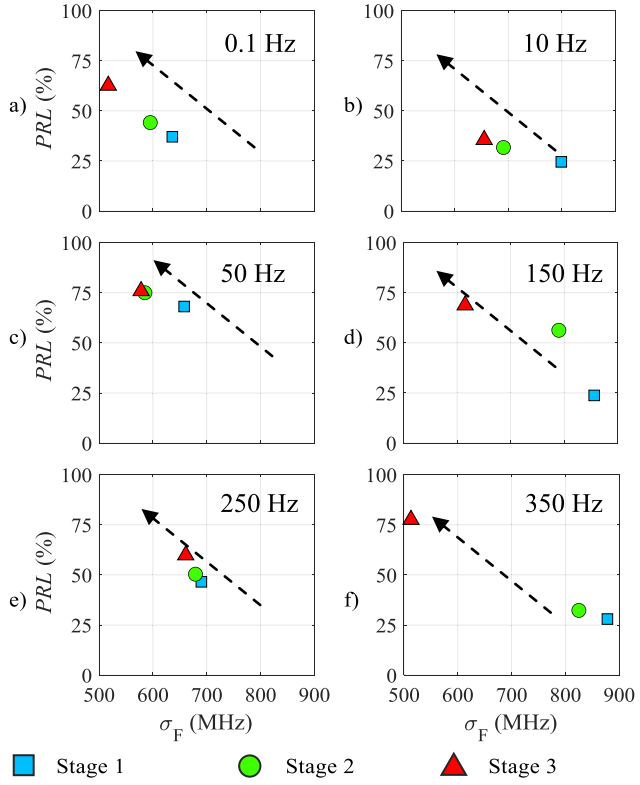

FIGURE 7. Proposed map for the six treeing-samples energized with different frequency: (a) 0.1 Hz 16 kV, (b) 10 Hz 14 kV, (c) 50 Hz 12 kV, (d) 150 Hz 12 kV, (e) 250 Hz 12 kV, (f) 350 Hz 12 kV.

As observed in Fig. 7, the response of the proposed $PRL - \sigma_F$ map is consistent for all the samples. Although the 50 Hz sample has a small variation between the second and third stage, this was due to the small growth of the tree between those two stages (from $l_{tree} = 0.82$ to $l_{tree} = 0.96$, as seen in Table 2).

The proposed map provides two main advantages when compared with the more traditional SPCT, TF and CT analyzed previously. First, the proposed $PRL - \sigma_F$ map allows a more consistent visualization of the relation between the values of the characteristic parameters of SCPT and TF techniques with respect to the tree length. Secondly, the new map becomes a more robust and reliable map since parameters *PRL* and σ_F complement each other: On the one hand, *PRL* parameter has the advantage of being sensitive to electrical tree growth at the expense of depending on the user-selection of the low- and high-frequency bands. On the other hand, the equivalent bandwidth σ_F does not require a previous user-entry for its calculation and can detect frequency shifts of the energy content towards or away from $\omega = 0$. Thus, in case of mis-selection of low frequency bands in the calculation of *PRL*, σ_F will show variation and reasonable sensitivity with tree growth. Furthermore, the results of σ_F may indicate that the selection of the frequency bands could be corrected, if required, becoming a feedback in the selection process.

In terms of computation effort, there is not extra burden. Moreover, *PRL* and σ_F share the requirement of calculating the Fourier transform of the signal, which makes this proposed map efficient when calculating both *PRL* and σ_F together, instead of separately for PR and TF maps.

VII. CONCLUSION

This paper presented the application of Spectral Power Clustering Technique (SPCT), Time-Frequency (TF) maps and Chromatic Technique (CT) for the identification of electrical tree growth. These separation techniques are normally used for classification of types of PD and noise separation. In this paper, the techniques were explored in their ability of determining the stage of electrical tree growth, and thus, to become a potential tool for insulation diagnosis. It was found that the waveform of PD pulses varied with electrical tree growth, and thus, the use of these mapping techniques that characterize PD waveform can also characterize the progression of electrical trees. Specifically, SPCT and TF maps provided more satisfactory results than CT. Parameters related to frequency content of PD signal were sensitive to tree growth. *PRL* parameter from SPCT always increased as the tree grew, indicating that the proportion of energy in the low frequency band was increasing with tree propagation. There was found a consistent relation between *PRL* and tree length, which could be useful in lifetime prediction. Similarly, the equivalent bandwidth σ_F, a TF map parameter, showed a consistent tendency with tree growth: σ_F always decreased with tree evolution. Therefore, a new map using *PRL* and σ_F was proposed combining the benefits they proved in their respective maps (SPCT and TF). The proposed $PRL - \sigma_F$ map gives a more consistent and robust response to the different stages of tree growth, providing a reliable monitoring tool.

Future research can involve the evaluation and comparison of these techniques with other available techniques, in terms of their capability of identifying the state of progress of tree growth.

REFERENCES

[1] L. A. Dissado and C. Fothergill, *Electrical Degradation and Breakdown in Polymers*, 1st ed. London, U.K.: Peter Peregrinus, 1992.
[2] J. Lawson and W. Vahlstrom, "Investigation of insulation deterioration in 15 KV and 22 KV polyethylene cables removed from service—Part II," *IEEE Trans. Power App. Syst.*, vol. PAS-92, no. 2, pp. 824–835, Mar. 1973.
[3] X. Chen, Y. Xu, and X. Cao, "Nonlinear time series analysis of partial discharges in electrical trees of XLPE cable insulation samples," *IEEE Trans. Dielectr. Electr. Insul.*, vol. 21, no. 4, pp. 1455–1461, Aug. 2014.
[4] J. V. Champion, S. J. Dodd, and J. M. Alison, "The correlation between the partial discharge behaviour and the spatial and temporal development of electrical trees grown in an epoxy resin," *J. Phys. D, Appl. Phys.*, vol. 29, no. 10, pp. 2689–2695, Oct. 1996.
[5] F. H. Kreuger, *Partial Discharge Detection in High-Voltage Equipment*, 1st ed. London, U.K.: Butterworths, 1989.
[6] *High-Voltage Test Techniques—Partial Discharge Measurements*, IEC Standard 60270, 2015.
[7] A. J. Reid, M. D. Judd, R. A. Fouracre, B. G. Stewart, and D. M. Hepburn, "Simultaneous measurement of partial discharges using IEC60270 and radio-frequency techniques," *IEEE Trans. Dielectr. Electr. Insul.*, vol. 18, no. 2, pp. 444–455, Apr. 2011.
[8] R. Albarracín, J. Ardila-Rey, and A. Mas'ud, "On the use of monopole antennas for determining the effect of the enclosure of a power transformer tank in partial discharges electromagnetic propagation," *Sensors*, vol. 16, no. 2, p. 148, Jan. 2016.
[9] A. Cavallini, G. C. Montanari, F. Puletti, and A. Contin, "A new methodology for the identification of PD in electrical apparatus: Properties and applications," *IEEE Trans. Dielectr. Electr. Insul.*, vol. 12, no. 2, pp. 203–215, Apr. 2005.
[10] A. Cavallini, G. Montanari, A. Contin, and F. Pulletti, "A new approach to the diagnosis of solid insulation systems based on PD signal inference," *IEEE Elect. Insul. Mag.*, vol. 19, no. 2, pp. 22–30, Apr. 2003.
[11] P. Bidan, T. Lebey, and C. Neacsu, "Development of a new off-line test procedure for low voltage rotating machines fed by adjustable speed drives (ASD)," *IEEE Trans. Dielectr. Electr. Insul.*, vol. 10, no. 1, pp. 168–175, Feb. 2003.
[12] J. Ardila-Rey, J. Martínez-Tarifa, G. Robles, and M. Rojas-Moreno, "Partial discharge and noise separation by means of spectral-power clustering techniques," *IEEE Trans. Dielectr. Electr. Insul.*, vol. 20, no. 4, pp. 1436–1443, Aug. 2013.
[13] J. Ardila-Rey, M. Rojas-Moreno, J. Martínez-Tarifa, and G. Robles, "Inductive sensor performance in partial discharges and noise separation by means of spectral power ratios," *Sensors*, vol. 14, no. 2, pp. 3408–3427, Feb. 2014.
[14] J. A. Ardila-Rey, M. P. Cerda-Luna, R. A. Rozas-Valderrama, B. A. de Castro, A. L. Andreoli, and F. Muhammad-Sukki, "Separation techniques of partial discharges and electrical noise sources: A review of recent progress," *IEEE Access*, vol. 8, pp. 199449–199461, Nov. 2020.
[15] J. Ardila-Rey, J. Montaña, B. de Castro, R. Schurch, J. C. Ulson, F. Muhammad-Sukki, and N. Bani, "A comparison of inductive sensors in the characterization of partial discharges and electrical noise using the chromatic technique," *Sensors*, vol. 18, no. 4, p. 1021, Mar. 2018.
[16] F. Alvarez, J. Ortego, F. Garnacho, and M. A. Sanchez-Uran, "A clustering technique for partial discharge and noise sources identification in power cables by means of waveform parameters," *IEEE Trans. Dielectr. Electr. Insul.*, vol. 23, no. 1, pp. 469–481, Feb. 2016.
[17] L. Hao, P. Lewin, J. Hunter, D. Swaffield, A. Contin, C. Walton, and M. Michel, "Discrimination of multiple PD sources using wavelet decomposition and principal component analysis," *IEEE Trans. Dielectr. Electr. Insul.*, vol. 18, no. 5, pp. 1702–1711, Oct. 2011.
[18] K. Firuzi, M. Vakilian, V. P. Darabad, B. T. Phung, and T. R. Blackburn, "A novel method for differentiating and clustering multiple partial discharge sources using s transform and bag of words feature," *IEEE Trans. Dielectr. Electr. Insul.*, vol. 24, no. 6, pp. 3694–3702, Dec. 2017.
[19] R. D. Nimmo, G. Callender, and P. L. Lewin, "Methods for wavelet-based autonomous discrimination of multiple partial discharge sources," *IEEE Trans. Dielectr. Electr. Insul.*, vol. 24, no. 2, pp. 1131–1140, Apr. 2017.
[20] J. A. Ardila-Rey, R. Schurch, J. Montaña, A. A. Mas'ud, and N. M. Poblete, "Sensitivity assessment of power ratio maps due to variation of internal defects in solid insulation," in *Proc. Int. Symp. High Voltage Eng.*, 2019, pp. 1–5.
[21] M. Conti, A. Cavallini, G. C. Montanari, and F. Guastavino, "Identification of electrical tree growth in insulation systems by fuzzy logic techniques based on partial discharge acquisition," in *Proc. IEEE Int. Conf. Solid Dielectr. (ICSD)*, Toulouse, France, 2004, pp. 661–664.
[22] R. Vogelsang, B. Fruth, T. Farr, and K. Fröhlich, "Detection of electrical tree propagation by partial discharge measurements," *Eur. Trans. Electr. Power*, vol. 15, no. 3, pp. 271–284, May 2005.
[23] N. M. Chalashkanov, S. J. Dodd, L. A. Dissado, and J. C. Fothergill, "A comparison between PSA plots of partial discharges in needle voids and electrical trees," in *Proc. IEEE Int. Conf. Dielectr. (ICD)*, Montpellier, France, Jul. 2016, pp. 476–479.
[24] R. Sarathi, K. H. Oza, C. L. G. P. Kumar, and T. Tanaka, "Electrical treeing in XLPE cable insulation under harmonic AC voltages," *IEEE Trans. Dielectr. Electr. Insul.*, vol. 22, no. 6, pp. 3177–3185, Dec. 2015.
[25] P. Donoso, R. Schurch, J. Ardila, and L. Orellana, "Analysis of partial discharges in electrical tree growth under very low frequency (VLF) excitation through pulse sequence and nonlinear time series analysis," *IEEE Access*, vol. 8, pp. 163673–163684, Sep. 2020.
[26] R. Schurch, O. Munoz, and J. Ardila-Rey, "Spectral power analysis of partial discharges waveforms during electrical tree growth under different excitation frequencies," in *Proc. 21st Int. Symp. High Voltage Eng.*, Budapest, Hungary, 2019, pp. 899–907.
[27] X. Liang, "Emerging power quality challenges due to integration of renewable energy sources," *IEEE Trans. Ind. Appl.*, vol. 53, no. 2, pp. 855–866, Mar. 2017.
[28] X. Wang, X. Li, M. Rong, D. Xie, D. Ding, and Z. Wang, "UHF signal processing and pattern recognition of partial discharge in gas-insulated switchgear using chromatic methodology," *Sensors*, vol. 17, no. 12, p. 177, Jan. 2017.
[29] G. Robles, R. Albarracín, and J. M. Martínez-Tarifa, "Shielding effect of power transformers tanks in the ultra-high-frequency detection of partial discharges," *IEEE Trans. Dielectr. Electr. Insul.*, vol. 20, no. 2, pp. 678–684, Apr. 2013.
[30] G. Robles, J. Martínez-Tarifa, M. Rojas-Moreno, R. Albarracín, and J. Ardila-Rey, "Antenna selection and frequency response study for UHF detection of partial discharges," in *Proc. IEEE Int. Instrum. Meas. Technol. Conf.*, Graz, Austria, May 2012, pp. 1496–1499.
[31] G. Robles, J. Fresno, and J. Martínez-Tarifa, "Separation of radio-frequency sources and localization of partial discharges in noisy environments," *Sensors*, vol. 15, no. 5, pp. 9882–9898, Apr. 2015.
[32] J. M. Martínez, J. A. Ardila-Rey, and G. Robles, "Automatic selection of frequency bands for the power ratios separation technique in partial discharge measurements: Part I, fundamentals and noise rejection in simple test objects," *IEEE Trans. Dielectr. Electr. Insul.*, vol. 22, no. 4, pp. 2284–2291, Aug. 2015.
[33] J. Zhang, G. R. Jones, J. W. Spencer, P. Jarman, I. J. Kemp, Z. Wang, P. L. Lewin, and R. K. Aggarwal, "Chromatic classification of RF signals produced by electrical discharges in HV transformers," *IEE Proc.-Gener., Transmiss. Distrib.*, vol. 152, no. 5, pp. 629–634, 2005.
[34] H. Zheng, S. M. Rowland, I. Iddrissu, and Z. Lv, "Electrical treeing and reverse tree growth in an epoxy resin," *IEEE Trans. Dielectr. Electr. Insul.*, vol. 24, no. 6, pp. 3966–3973, Dec. 2017.
[35] R. Schurch, J. Ardila-Rey, J. Montana, A. Angulo, S. M. Rowland, I. Iddrissu, and R. S. Bradley, "3D characterization of electrical tree structures," *IEEE Trans. Dielectr. Electr. Insul.*, vol. 26, no. 1, pp. 220–228, Feb. 2019.

CARLOS MADARIAGA (Student Member, IEEE) received the B.Sc. and M.Sc. degrees in electrical engineering from the Pontificia Universidad Católica de Valparaíso, Chile, in 2017 and 2020, respectively. He is currently pursuing the Ph.D. degree with the University of Concepcion, Chile. He was granted a scholarship to pursue his Ph.D. studies from the National Research Development Agency, in 2020. His research interests include modeling, design, and optimization of electromechanical devices.

ROGER SCHURCH (Member, IEEE) received the degree in electrical engineering from Federico Santa Maria Technical University (UTFSM), Valparaiso, Chile, in 2006, and the Ph.D. degree from The University of Manchester, in 2014. He was a High-Voltage Equipment Analyst with Transelec Transmission Company, before joining UTFSM, as Lecturer, in 2008. He currently re-joined UTFSM as an Assistant Professor. His research interests include electrical trees and partial discharges and insulation diagnostics of power systems plant.

JORGE ARDILA-REY (Member, IEEE) was born in Santander, Colombia, in 1984. He received the B.Sc. degree in mechatronic engineering from the Universidad de Pamplona, Pamplona, Colombia, in 2007, the Specialist Officer degree in naval engineering from Escuela Naval Almirante Padilla, Cartagena, Colombia, in 2008, and the M.Sc. and Ph.D. degrees in electrical engineering from the Universidad Carlos III de Madrid (UC3M), in 2012 and 2014, respectively. He was an Automatic Control Engineer of ARC Almirante Padilla, from 2008 to 2010. From 2010 to 2014, he worked with the Department of Electrical Engineering, High-Voltage Research and Tests Laboratory (LINEALT), UC3M. He is currently working as a Professor with the Department of Electrical Engineering, Universidad Técnica Federico Santa María, Santiago, Chile. His research interests include partial discharges, insulation systems diagnosis, and instrumentation and measurement techniques for high-frequency currents.

OSVALDO MUÑOZ was born in Quillota, Chile, in 1994. He received the B. Sc. degree in electrical engineering from Universidad Técnica Federico Santa María (UTFSM), Valparaíso, Chile, in 2017, where he is currently pursuing the M.S. degree in electrical engineering. His thesis work is about partial discharges in electrical trees under harmonic frequencies characterized by partial discharge waveforms.

SEBASTIAN FINGERHUTH (Member, IEEE) received the bachelor's degree (E.Eng.) from the Pontificia Universidad Católica de Chile (PUC), in 2003, and the Ph.D. degree (Dr.-Ing.) in acoustics from RWTH Aachen University, Germany, in 2009. As a Researcher and an Engineer, he worked in acoustic, psychoacoustic, vibrations, and noise reduction projects with RWTH Aachen University, Germany. He is currently a full-time Professor with the School of Electrical Engineering, Pontificia Universidad Católica de Valparaíso. He is working in projects in areas such as acoustics, structural vibration, instrumentation, sensors, and signal processing. He is a member of the German Acoustic Society (DEGA) and the American Society of Acoustics (ASA).